Proceedings World Geothermal Congress 2005
Antalya, Turkey, 24-29 April 2005

Modelling the Deep Geothermal System of the Uenotai Reservoir

Stephen P. White[1], Takashi Okabe[2], Tatuya Sato[2], Masatake Sato[2], Takahiro Shiga[2], Yoshinobu Takahashi[3]

[1]Applied Mathematics, Industrial Research Limited, P.O. Box 31310, Lower Hutt, New Zealand

S.White@irl.cri.nz

[2]Geothermal Energy Research and Development Co. Ltd, 11-7Kabuto-cho, Nihonbashi, Chuo-ku, Tokyo 103-0026, Japan

[3]Akita Geothermal Energy Co., Ltd, Yuzawa-shi, Akita-ken, 019-0404, JAPAN

Keywords: Reservoir Modelling, water-rock interaction, reactive chemical transport NEDO

ABSTRACT

The Uenotai geothermal field lies 380-km northeast of Tokyo in the Akita Prefecture The reservoir has been in operation since March 1994, operated by the Akita Geothermal Energy Co. Ltd. and supplies steam to the power plant operated by Tohoku Electric Power Company Inc. Currently 28.8 MW of electricity is generated.

In this work we have used reactive chemical transport modelling to calculate the rock alteration products and chemistry of the Uenotai reservoir and test the effect of different permeability structures at depth on the calculated pattern of rock alteration. Where agreement between observation and calculation is better for some deep permeability structures than others, then this provides some evidence for choosing a particular permeability structure as being a good representation of the nature of the permeability at depth.

This project was conducted as one of the Geothermal Development Promotion Survey Projects of NEDO.

1. INTRODUCTION

The Uenotai geothermal field lies 380-km northeast of Tokyo in the Akita Prefecture (Figure 1). The reservoir has been in operation since March 1994, operated by the Akita Geothermal Energy Co. Ltd. and supplies steam to the power plant operated by Tohoku Electric Power Company Inc. Currently 28.8 MW of electricity is generated.

This paper describes the development of a numerical model of the geothermal system beneath the currently produced area of the Uenotai reservoir. The work is part of a NEDO sponsored initiative “Deep-Seated Geothermal Resources Survey”. The final goal of the project is promoting the development of deep-seated geothermal resources (below approximately 2,000m in depth).

The model described here extends to a depth of 4.5 kilometers below the ground surface and models not only the flow of water and heat in the reservoir, but also the major chemical species and several water-rock alteration products. These extra complications are introduced in an attempt to improve our understanding of the deep permeability structure beneath the explored reservoir.

Magmatic intrusions are obvious heat sources for geothermal fields. Perhaps the most thoroughly studied intrusion is that at the Kakkonda reservoir in Japan (Sasada *et al.* 1998). The chemistry and rock alteration of this system was modelled using the reactive chemical transport simulator CHEM-TOUGH2 (White 1998, Sato et al. 2000). Although less well studied, a diorite intrusion was also intersected during the drilling of geothermal well NM4 in the Ngatamariki field, New Zealand. Again the rock alteration and chemistry above this system has been modelled using CHEM-TOUGH2 (White and Christenson 1998,2000). The modelling of these systems demonstrated that the chemistry and rock alteration above an intrusion can be modelled in some detail and the work on Kakkonda in particular showed that assumptions about deep permeability alter the calculated shallow rock alteration.

The aim in this work is to use reactive chemical modelling to calculate the rock alteration products and chemistry of the Uenotai reservoir and test the effect of different permeability structures at depth on the calculated pattern of rock alteration. If the agreement between observation and calculation is better for some deep permeability structures than others then this provides some evidence for choosing a particular permeability structure as being a good representation of the nature of the permeability at depth.

2. GEOLOGY OF THE UENOTAI AREA

The Uenotai geothermal field is in Akita prefecture, in the northern part of Honshu Island, Japan (Figure 1). Gentle domes and basins characterize the geological structure of this area. The Uenotai power plant is located to the North of the Kamuro Mountains and the Onikobe power plant is located to the East of the mountains. These power stations are either on the rim of, or inside the basins.

The Ohyu backbone mountains run along the east of the area. The Pre-Tertiary rocks forming the basement underlying the area consist of the Neogene, the Quaternary and the intrusive rock in the Neogene. Pre-Tertiary rocks consist of greenschist, serpentinite and granodiorite. The Neogene is divided into Doroyu, Minasegawa and Sanzugawa formations. The Quaternary rocks consist of the Kabutoyama formation and the Takamatudake-volcanic rocks. The intrusive rocks consist of Neogene-granite, dacite, andesite and dolerite. The primary faulting runs mainly in a NW-SE direction, NE-SW direction faults are secondary. Geothermal indications such as alteration zones, hot springs and fumarole zones are present along the NW-SE directional faults.

The reservoir within the Uenotai project area is formed primarily by a horst block consisting mainly of Tertiary intrusive rock, pre-Tertiary granitic and metamorphic rocks and lava.

While *et al*.

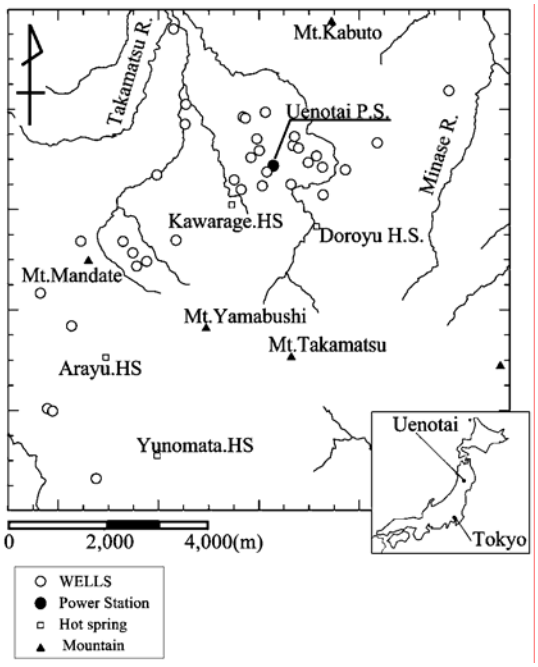

Figure 1:Location of the Uenotai geothermal reservoir.

3. CONCEPTUAL MODEL

A conceptual model, developed mainly from the geochemistry of the region, of the Uenotai project area has been described by Robertson-Tait *et al*. (1990).

They identified seven distinct water types in the Uenotai area

1. Type 1 is found on the surface and in shallow cool aquifers.

2. Type 2 is the deep, high temperature water found over most of the production area. In the production area it has chloride concentrations between 500 ppm and 150 ppm, decreasing from south to north. It is believed to have evolved from a parent fluid of about 650 ppm chloride.

3. Type 3 is a high temperature chloride water formed from the mixing of conductively cooled type 2 water with type 1 water. This water contains higher sulphate than the type 2 water, perhaps through the dissolution of anhydrite or possibly through the oxidation of H_2S in the type 2 water by dissolved oxygen in the type 1 water.

4. Type 4 is a dilute, high temperature bicarbonate water overlying the type 2 water in the main reservoir. This water is formed by the dissolution of non-condensable gases from the deep fluid in type 1 water.

5. Type 5 is a high chloride water (up to 5000 ppm) found in a small area to the south of the field. (This area is outside the modelled region.)

6. Type 6 is acid sulfate water found at several thermal features south of the project area on the Takamatsu high.

7. Type 7 is acid chloride-sulphate water found at Kawarage and Doroyu hot springs on the Takamatsu high.

The interaction of these waters is shown in Figure 2, taken from Robertson-Tait *et al*. (1990). They conclude that the Takamatsu and Minase waters are probably heated by a small local intrusion beneath the Takamatsu high. They also suggest another (less likely) possibility of an acid high chloride water sourced deep beneath the volcanic arc rising under the Takamatsu high and boiling to produce HCl that forms the acid chloride springs. The productive reservoir is mainly contained in a horst block composed of Tertiary intrusives, pre-Tertiary granitic and metamorphic rocks and lava. Permeability is primarily provided by fractures in the structural high and is bounded by normal faults. The fractured permeable reservoir rock is bounded by low permeability rock.

The numerical model described in this work is based on the conceptual model of a small local intrusion beneath the Takamatsu high. A plan view of the region showing the assumed location of the heat source and the region covered by the numerical model is shown in Figure 2.

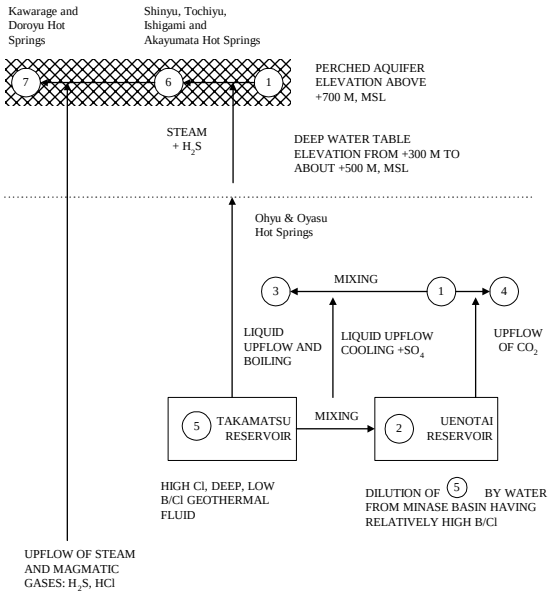

Figure 2: Conceptual model of the source of fluids in the Uenotai reservoir (from Robertson-Tait *et al.* 1990, Figure 7)

Unfortunately there is no obvious symmetry in this conceptual model that would allow a two-dimensional model of the system to be developed. The location of the heat source in the south and recharge water from the Minase basin in the north force us to use a full three-dimensional model to represent the expected fluid-flow paths in the reservoir. This has meant the chemical model is simpler than that used for Kakkonda (Sato et al 2000) as computer time requirements increase rapidly with increasingly complex chemical models and the extension from two to three dimensions.

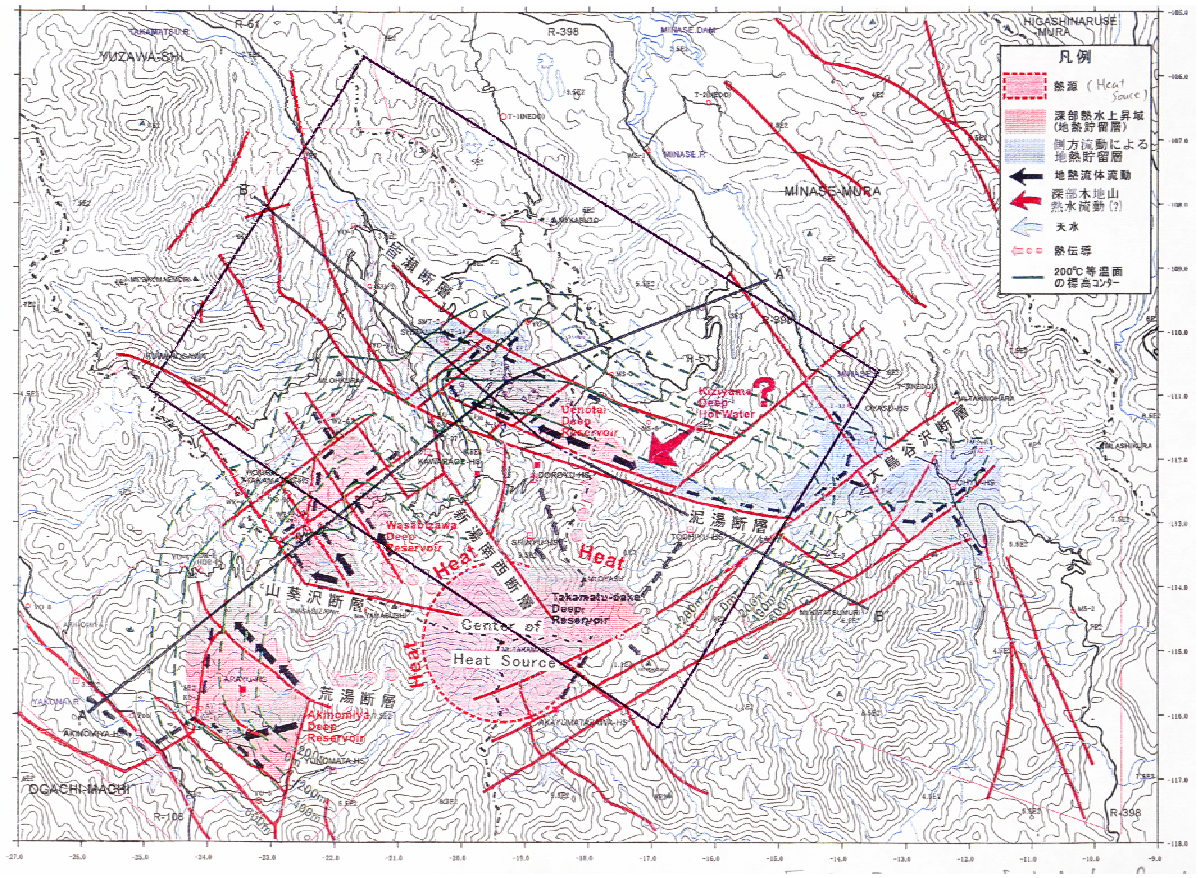

Figure 3: Plan view of the Uenotai area with the area modelled shown as a black rectangle.

4. NUMERICAL MODEL

4.1. Model description

The model is a three-dimensional integrated finite difference model based on an existing model. In the earlier TOUGH2 model a large effort was put into optimizing the parameters used for the shallow reservoir in this model and it is believed to be a good representation of the currently developed reservoir. In this work we take the shallow reservoir parameters as fixed and concentrate only on estimating the parameters in the deep reservoir.

Some changes to the boundary conditions and block structure of the shallow model have been made to this model to meet the needs of this study.

1. The surface boundary condition has been changed so that there may be some recharge water to the reservoir from the surface. This was achieved by setting the permeability of the 'AIR' block to be non-zero.

2. The horizontal block structure has been simplified. This was necessary as the computational demands of chemical modelling are large and it was not possible to include all the detail of the original GERD model. The grid structure of the new model is shown in Figure 4.The model has been extended to a greater depth than the original model. It now reaches from the surface at 600 masl to –4000 masl. The layer structure of the new model is shown in Figure 5.

3. Above -1500 masl the permeability structure is identical to the original model. Below this depth the reservoir is divided into four different rock types. These rock types are shown in Figure 6.

The simplified grid is shown in Figure 4 and the vertical structure in Figure 5. As can be seen the detail is still greater in the production area of the field but has been reduced to make the chemical modelling possible.

4.2. Parameters of the deep reservoir

Permeability

No wells have been drilled deeper that about 1000 meters below sea level (mbsl) so the model below this depth is somewhat speculative. The approach adopted is to assume four different rock types below the area modelled by the existing reservoir model and adjust the parameters of these to match the observed temperature distribution of the reservoir. The location of the four rock types is shown in Figure 5, they form approximately concentric rings centered beneath the Uenotai reservoir. In keeping with the Robertson-Tait *et al.* (1990) conceptual model the outermost ring is assumed to have a low permeability (10^{-19} m^2). The permeability of rocks within this low permeability boundary together with heat and mass flows across the bottom of the model are adjusted to provide a match to the shallow temperatures.

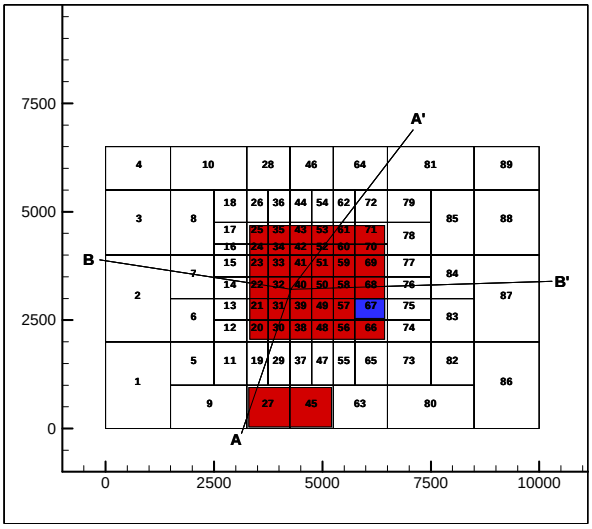

Figure 4: Mesh layout of model and base boundary conditions. The blue area shows the location of inflow of mixed type 5 and Minase basin water. The red area shows the region of high conductive heat input.

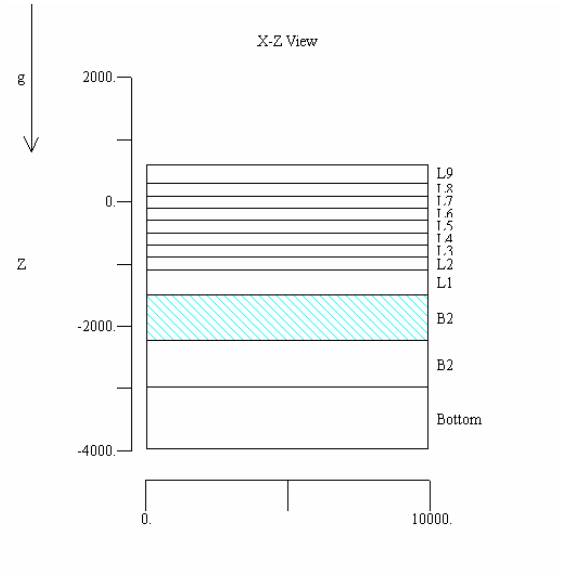

Figure 5:Vertical structure of the model. Layers L1-L9 represent the original model.

Permeabilities were adjusted using ITOUGH2 to automate the adjustment of permeabilities and heat flows in matching to these temperatures. There were some problems with this approach. These were not because of problems with ITOUGH2 but rather with the way the supercritical module (Kissling and White, 1999) dealt with two-phase subcritical to supercritical transitions. Considerable effort has been devoted to modelling these transitions correctly and although the problem has not been completely solved we were able to calculate parameters for the deep reservoir that provided a reasonable match to shallow temperatures.

4.3. Boundary Conditions at the Base

Several different scenarios were investigated with different boundary conditions at the base of the model; these are described in the results section. In the base case energy flow into the system across the bottom boundary is 13 MW.

This energy flow is supplied by conduction (11.8 MW) and by a high enthalpy (2000 kJ/kg) source fluid flowing in at a rate of 0.6 kg/s providing a further 1.2MW. This source fluid contains dissolved CO_2, H_2S and HCl gases. In terms of the conceptual model it represents diluted type 5 water and forms the parent fluid for the type 2 water found over most of the Uenotai production reservoir.

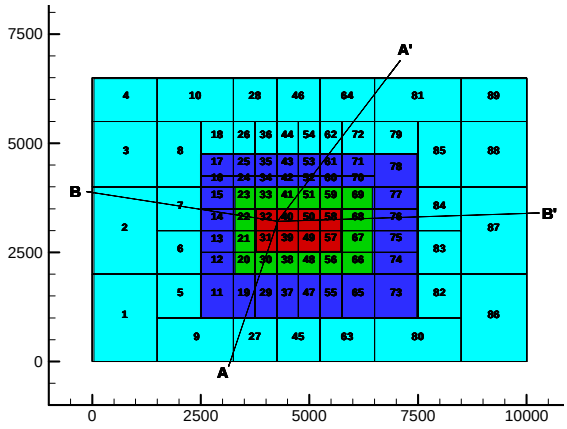

Figure 6: Permeability structure assumed at depth. The innermost region (coloured red) is referred to as D 3, then the surrounding regions as D 2 (green), D 1 (blue) and Outside (cyan).

4.4. High temperature permeability

Measurements made in well WD1 (Doi *et a.l* 1998) at the Kakkonda field, make it clear that basement rock with a temperature above 380-400^{o} C has very low permeability and the hydrothermal system does not penetrate rocks above this temperature. This effect is ascribed to the rock undergoing an elastic-plastic transition. Once rock has become plastic it will 'flow' under a pressure gradient effectively closing the micro-fractures that provide permeability. White and Mroczek (1998) review the mechanisms for permeability creation and destruction and this paper provides more references on this effect. To take account of this effect we model permeability as reducing linearly over the temperature range 400^{o}C – 420^{o}C. Above 420^{o}C the permeability is set at a fixed value of 10^{-3} times the low temperature value.

4.5. Geology and Geochemistry

While the general nature of the geology has been investigated and a good description of rock types in the area is available, there is little detailed information on the composition of the rocks making up the reservoir. A single composition is assumed for the whole modelled region. We assume the original rock in the reservoir is composed of a mixture of (Na, K, Ca) feldspars and quartz. This is a reasonable approximation to the rock types found in the reservoir and contains the main chemical elements found in the water of the reservoir. Of the measured anions in the reservoir only magnesium and iron are not present in this assumed rock assemblage. The measured amounts of these are very small compared to those included in the modelling.

Modelling the transport of reactive chemicals is a computer intensive activity, and requires that a balance be struck between chemical complexity and calculation time. For the rock assemblage chosen we need to include the reservoir component species, H_2O, H^+, Cl^-, $SO_4^{=}$, HCO_3^-, HS^-, SiO_2,

Al^{+++}, Ca^{++}, K^{+} and Na^{+}. These fluid components allow the modelling of reactions between the main magmatic volatiles (CO_2, H_2S, HCl) and the most common rock-forming minerals (albite, anorthite, K-feldspar and quartz).

The rock alteration minerals observed at Uenotai are Montmorillinite, Chlorite, Kaolinite, Mordenite, Laumontite, Wairakite Analcime, Quartz, Gypsum, Anhydrite, Calcite, Epidote, Albite, Pyrite, Stilbite and Heulandite.

Those that are rare or contain iron or magnesium have not been included in the calculations. Others, for example Montmorillinite, are not single minerals but a mixture of a number of different minerals and, without detailed information about the constituent minerals, such minerals cannot be included in the calculation. Finally, for some of the observed minerals no thermodynamic data is available and these are also eliminated from the calculation.

The set of rock alteration minerals included in the final calculation is Laumontite, Wairakite, Quartz, Calcite, Anhydrite and Albite together with the initial mineral assemblage consisting of Albite, Anorthite, K-Feldspar and Quartz.

Thermodynamic data

The SOLTHERM database (Reed 1982) provides equilibrium constants as a function of temperature for all the reactions considered in this work up to a temperature of 350°C. It appears none of the widely available chemical databases provides data above this temperature explicitly. The program SUPCRT92 (Johnson *et a.l* 1992) and associated databases provide a theoretical prediction of equilibrium constants for almost all the reactions of interest at temperatures up to 415° C. There is excellent agreement between theoretical predictions of SUPCRT92 and the SOLTHERM database in regions where they overlap.

It is not possible to calculate the activity coefficients for charged species near the critical point of water. The approach we have taken is to use the values for equilibrium constants and activity coefficients for 350°C for all temperatures greater than 350°C.

4.6. Modelling Software

For this work we have used a version of TOUGH2 (Pruess 1991) that has been modified to include the transport of reacting chemicals (White 1995). The original code was capable modelling temperatures up to 350°C and pressures up to 100 MPa. This has been extended to temperatures up to 800°C but the pressure limit of 100 MPa remains (White and Mroczek 1998).

We have ignored the solubility of all neutral aqueous species in the gas phase even though it may be significant between 360 - 374°C with pressures on the saturation line. Carbon dioxide and hydrogen sulfide gases are included in the simulation as is the effect they have on the saturation pressure of water.

5. RESULTS

Three scenarios are presented and the parameters for these are given in Table 1. **Scenario 1** assumes poor permeability at depth and energy is transferred to the field primarily by heat conduction. It was necessary to reduce the rate of fluid flow at the base in this scenario otherwise the calculated pressures exceeded the limits of the software (1000 bars). This pressure represents a pressure about 600 bars in excess of hydrostatic. If pressures did reach this level it is expected that permeability would be created through host rock failure and the assumption of low permeability would not be correct. **Scenario 2** had high permeability at depth and used the permeabilities calculated using ITOUGH2. Inspection of the temperature distribution calculated for this scenario shows that it is too cool in the area of the Uenotai reservoir although over the full area of the model it gives a reasonable match. **Scenario 3** is a modified version of scenario 2 with permeabilities and heat flow adjusted to improve the match to temperatures in the productive area of the Uenotai reservoir.

Table 1: Heat and mass flows into the base of the reservoir assumed for the three scenarios.

Parameter	Scenario 1	Scenario 2	Scenario 3
D1 Permeability (m^2)	1.0×10^{-17}	3.8×10^{-16}	3.8×10^{-16}
D2 Permeability (m^2)	1.0×10^{-17}	5.8×10^{-14}	1.9×10^{-15}
D3 Permeability (m^2)	1.0	3.9×10^{-15}	1.9×10^{-15}
Outside Permeability (m^2)	1.0×10^{-19}	1.0×10^{-19}	1.0×10^{-19}
Conduction across base	11.8 MW	11.8 MW	12.7 MW
Convection across base	0.3 MW	1.2 MW	1.5 MW

In the interests of keeping to the page limit, results are presented only for scenarios one and three. We present contours of selected variables along two sections of the model (marked A-A' and B-B' in Figure 4). These sections were chosen as they correspond to sections used to present measured data.

Only a subset of the available data is presented, there are over 50 variables that could be contoured on these sections and obviously it is not practicable to present so much data. Data chosen for contouring are Temperature, pH and the location of rock alteration products Calcite, Laumontite and Wairakite.

These water-rock alteration products were chosen because they appear at different levels in a number of the wells and thermodynamic data is available on their solubility.

Figures 7 and 8 show the observed location of Laumontite and Wairakite taken from well drilling reports. The data from these figures are used to estimate the location of a Wairakite – Laumontite transition surface. The solubilities of these minerals are such that, for a given pH, in high temperature regions Wairakite should be present and in cooler regions Laumontite. This is generally true of the data shown in Figures 7 and 8. Taking the shallowest depth where Wairakite is observed and the deepest depth observed for Laumontite, an estimate of the depth of this transition is obtained.

Figures 9 and 14 show the calculated temperatures for scenario 1. These form an interesting contrast with those shown in Figures 22 and 27 (scenario 3). All scenarios have a similar temperature distribution at shallow levels although there is some variation in temperature between them with scenario 3 the hottest at shallow levels and scenario 1 the coolest. Scenario 3 appears to be the best match to observed temperatures in the Uenotai reservoir at shallow levels. At

depth, scenario 1 has peak temperatures over 800°C, scenario 2, 380°C and scenario 3, 390°C. It is interesting to compare these temperatures with those calculated by Shiga *et al*. from heat flow estimates. They estimate an upperbound on temperatures at –4000 m above sea level of 650°C and a lower bound of 480°C.

The bottom layer temperatures in this work are calculated at –3500 m above sea level so cannot be compared directly with Shiga *et al*. measurements but scenario 1 is certainly too hot. Scenarios 2 and 3 may reach 480°C at a depth of -4000 m above sea level.

There is some variation in calculated pH contours shown between the three scenarios (Figures 10, 23 and 28) but insufficient measured data was available to favor one scenario over another.

The location of the Laumontite-Wairakite interface is shown in Figures 12, 17, 25 and 30.

6. CONCLUSIONS

A three-dimensional model of the Uenotai geothermal reservoir has been developed that includes sufficient chemical components to calculate water-rock interaction products in the reservoir. Three different assumptions about deep permeability have been tested using this model. One of these scenarios (scenario 1) provides a poor match to observed water-rock interaction products and calculates temperatures at depth that exceed the estimated upper bounds calculated by Shiga *et al*. (2000).

One of the reasons for the high temperatures found in scenario 1 is the assumption of a temperature dependant permeability for the reservoir. The effect of the parameters chosen to specify the temperature dependence mean that permeability is reduced to almost zero for temperatures above 425°C. This choice of parameters is based on experience of the Kakkonda reservoir but may not be applicable at Uenotai.

The scenario that best seems to match observation has a large region (2.5 km × 1km) with a permeability of 2×10^{-15} m^2 beneath the existing reservoir. There may however be many other distributions of permeability that also give a reasonable match to the observed shallow rock alteration and temperatures. For example the permeability may be in just a few small high permeability regions.

The work does support a model that has convective flow to a considerable depth beneath the existing reservoir as the model with no convective flow (scenario 1) has a poor match to observation.

With more chemical data (sufficient to draw contours of reservoir pH and Cl^- for example) it may be possible to refine the model further.

7. REFERENCES

Doi N., Kato O., Ikeuchi K., Komatsu R., Miyazaki S.-I., Akaku K.,and Uchida T. (1998) Genesis of the plutonic-hydrothermal systemaround Quaternary granite in the Kakkonda geothermal system, Japan. *Geothermics* **27,** 663–690.

Johnson J.W., Oelkers, E.H., Helgeson, H.C., 1992, SUPCRT92: A software Package for Calculating the Standard Molal Thermodynamic Properties of Minerals, Gases, Aqueous Species and Reactions from 1 to 5000 Bar and 0 to 1000° C. *Computers & Geosciences* 18, 7, (1992)

Kissling W.M., and White, S.P. 1999, Supercritical TOUGH2 – Code description and Validation. Industrial Research Limited Report 905. (1999)

Pruess, K., 1991, TOUGH2 - A general-purpose numerical simulator for multiphase fluid and heat flow *Rep* LBL-29400, Lawrence Berkeley Lab., Berkeley, Calif.

Reed, M.H. (1982): Calculation of multi-component chemical equilibria and reaction processes in systems involving minerals, gases and an aqueous phase. *Geochim. et Cosmo. Acta* **46** 513-528

Robertson-Tait, A., Klein, C.W., McNitt, J.R., Naka, T., Takeuchi, R., Iwata, S., Saeki, Y. and Inoue, T. (1990) Heat source and fluid migration concepts at the Uenotai geothermal fields, Akita prefecture, Japan. *Geothermal resource Council Transactions*, Vol. 14, Part II, August 1990.

Sasada, M., Doi, N., Muffler, L.J., Hedenquist, J.W.:Deep geothermal Systems Japanese National project at Kakkonda. *Special issue Geothermics* 27, 5/6 1998

Sato, M. White, S. Osato, K. Sato, T. Okabe, T. Doi, N. Koide, K: *Modeling of chemistry and rock alteration at a Deep-seated Geothermal Field* Proc. 25th Stanford Geothermal Workshop (2000).

Shiga, T., Sato, S., Sato, T., Okabe, T., Osato, K., Takahashi, Y., Inque, T., White, S.P., Koide, K: Estimation of deep reservoir temperature distribution using stochastic methods in the Uenotai geothermal field. *Proc 21st New Zealand Geothermal Workshop* 2000

White, S.P.:Multi-phase Non-isothermal Transport of Systems of Reacting Chemicals, Water Resources Res. Vol 31 No. 7, pp. 1761-1772, 1995.

White, S.P., Mroczek, E: Permeability changes during the evolution of a geothermal field due to the dissolution and precipitation of quartz, TIPM, 33(1-2), pp. 81-101, 1998.

White, S.P., Christenson, B.W.: Modelling the alteration halo of a diorite intrusion. Proc. 20th New Zealand Geothermal Workshop. 1998

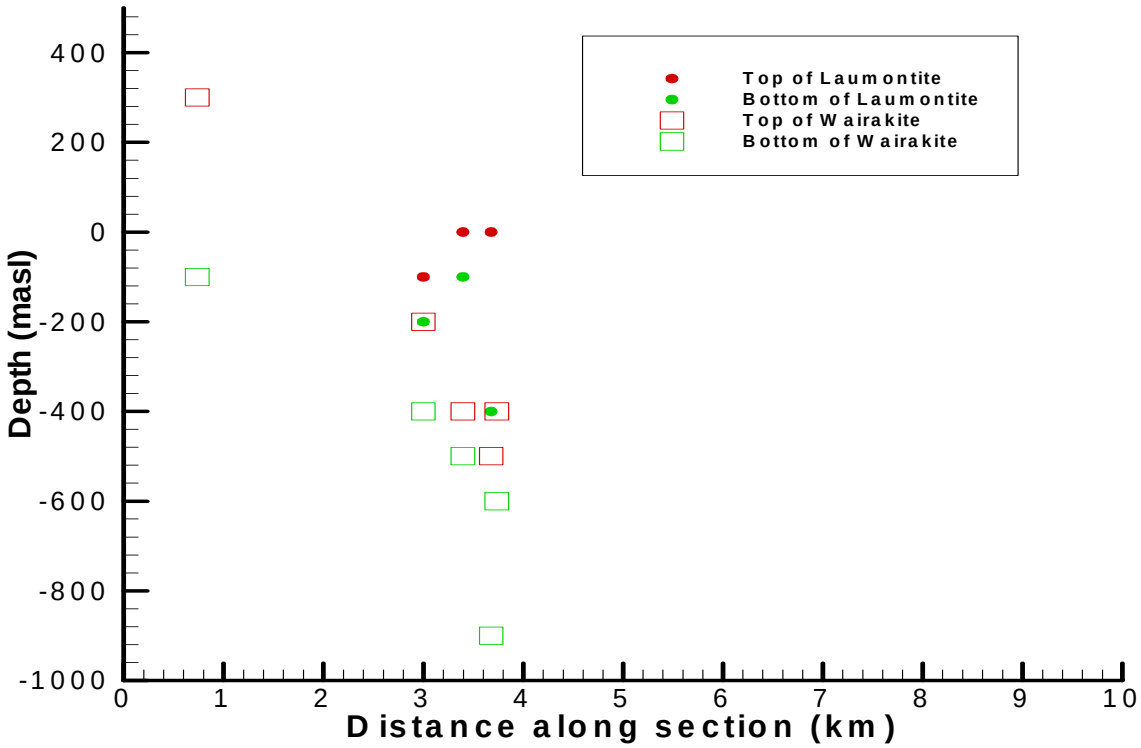

Figure 7:Observed regions of rock alteration along section A-A'. The section begins at well WZ2 (at zero distance).

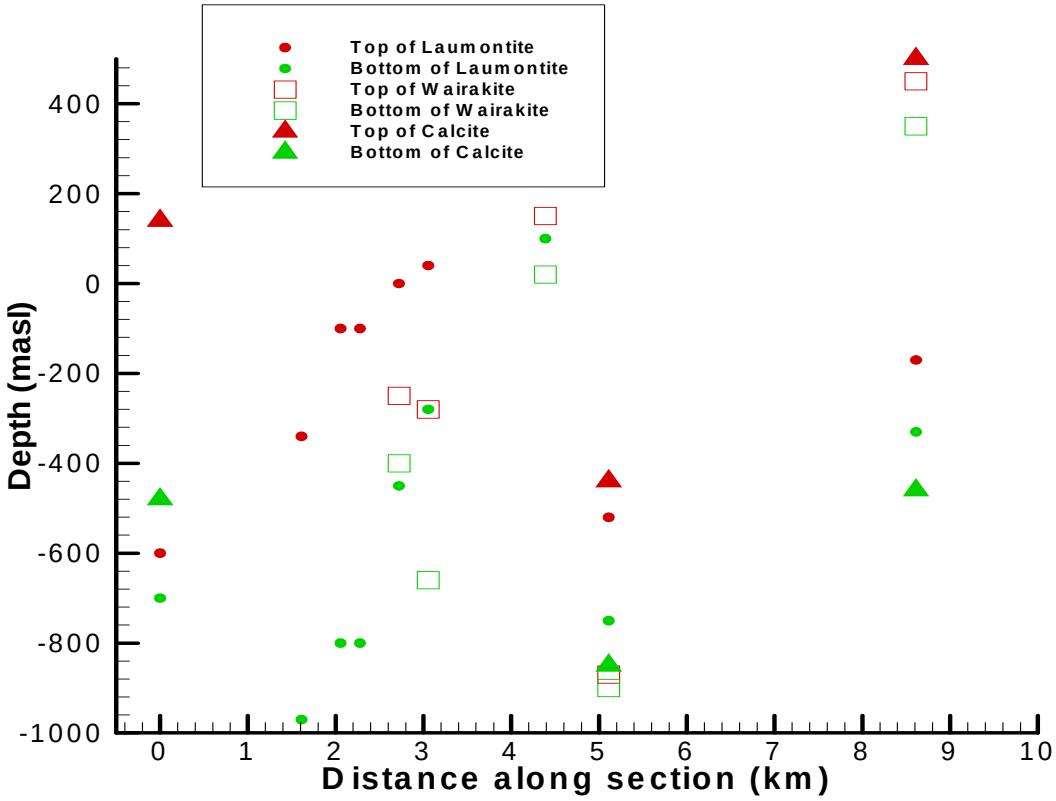

Figure 8:Observed regions of rock alteration along section B-B'. The section begins at well YO1 (at zero distance)

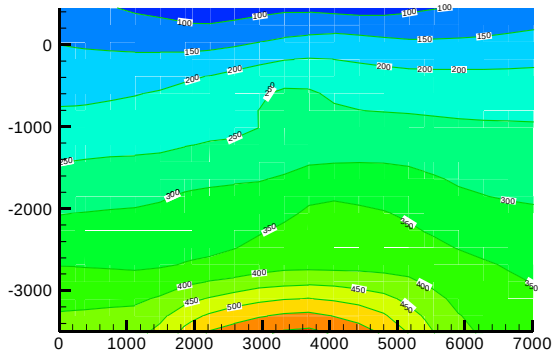

Figure 9: Temperature contours along section A-A' of Figure 4, scenario 1.

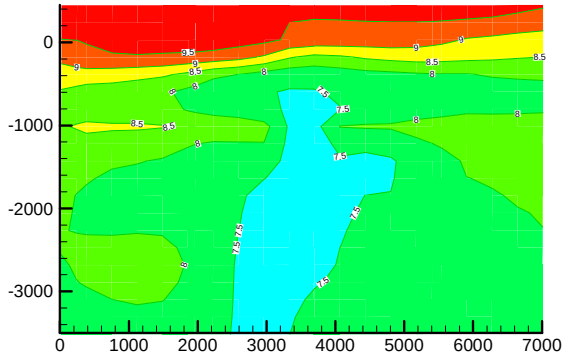

Figure 10: pH contours along section A-A' of Figure 4, scenario 1.

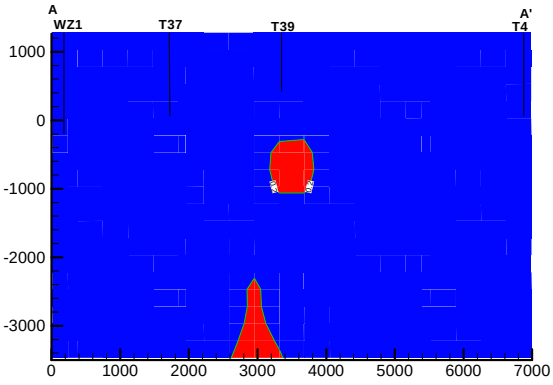

Figure 11:Regions of calcite deposition along section A-A' of Figure 4, scenario 1.

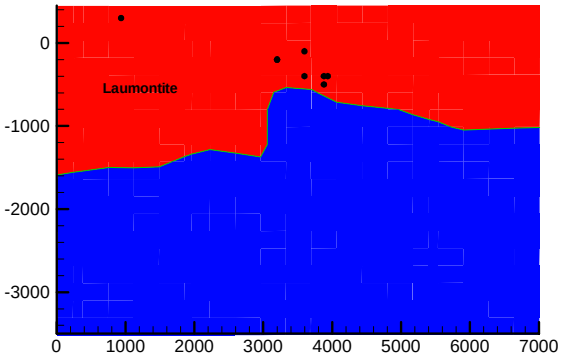

Figure 12: Regions of Laumontite deposition along section A-A' of Figure 4, scenario 1. The solid circles represent the lowest level of Laumontite alteration estimated from drillholes.

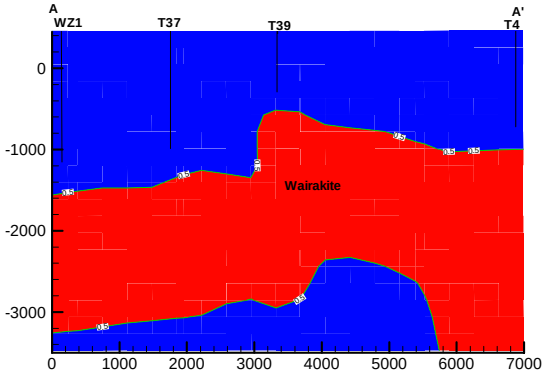

Figure 13: Regions of Wairakite deposition along section A-A' of Figure 4, scenario 1

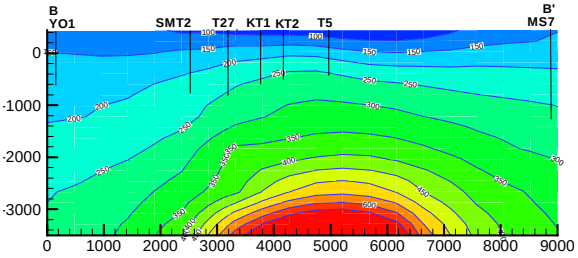

Figure 14: Temperature contours along section B-B' of Figure 4, scenario 1.

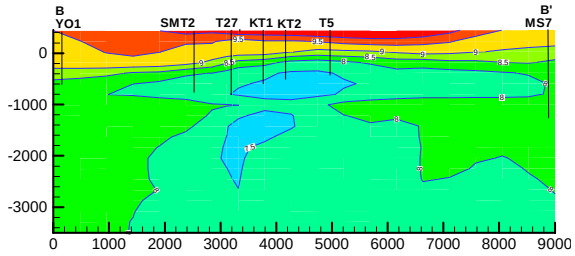

Figure 15: pH contours along section B-B' of Figure 4, scenario 1

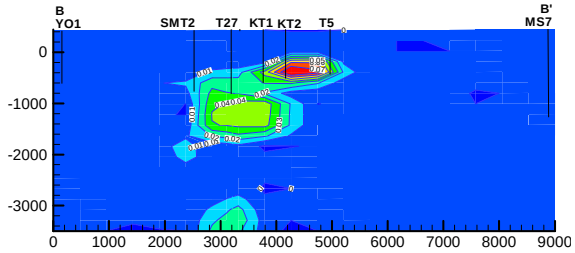

Figure 16: Calcite contours along section B-B' of Figure 4, scenario 1 (units are moles/dm^3 of rock)

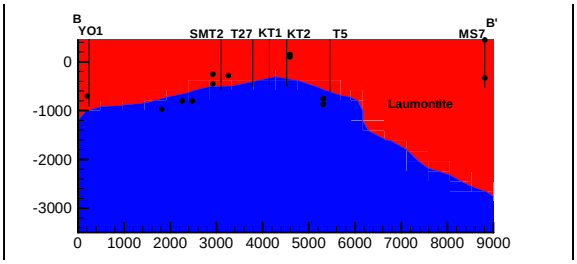

Figure 17: Location of Laumontite deposition along section B-B' of Figure 4, scenario 1. Solid circles represent maximum depth of Laminate, estimated from borehole data.

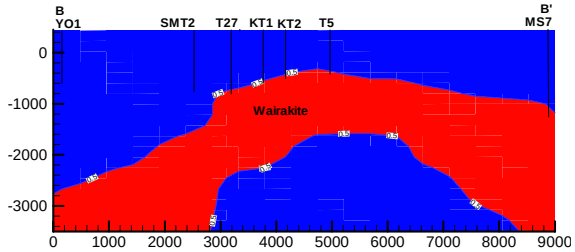

Figure 18: Location of Wairakite deposition along section B-B' of Figure 4, scenario 1.

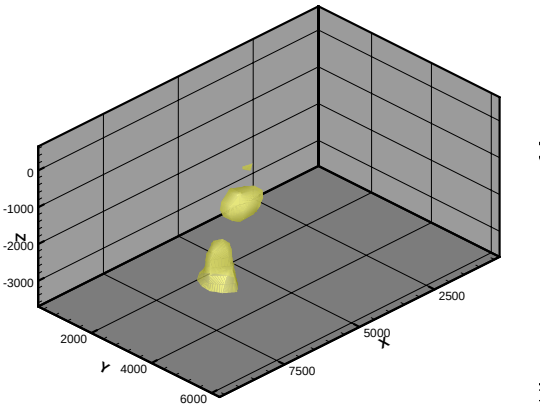

Figure 19:Location of calcite deposition, scenario 1.

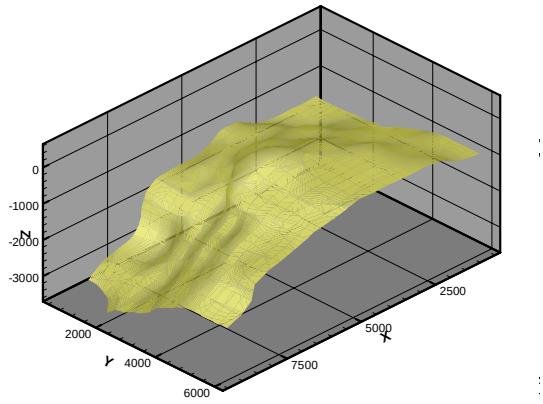

Figure 20: Lower surface of Laumontite over reservoir, scenario 1.

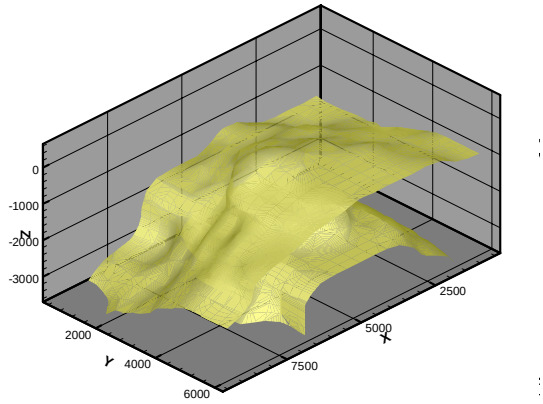

Figure 21: Upper and lower surfaces of Wairakite alteration, scenario 1.

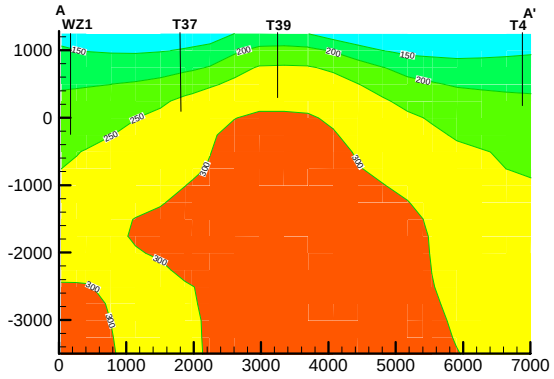

Figure 22:Temperature contours along section A-A' of Figure 4, scenario 3.

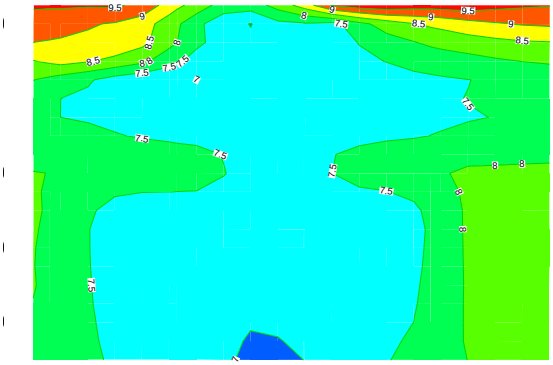

Figure 23:pH contours along section A-A' of Figure 4, scenario 3.

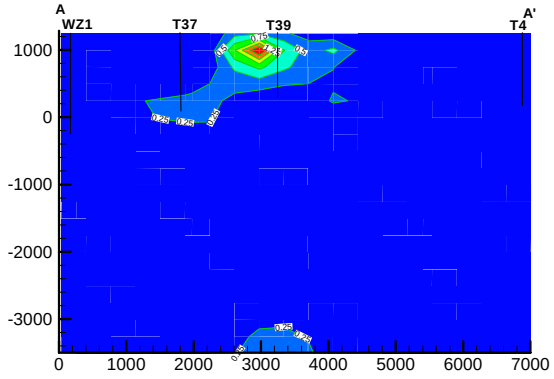

Figure 24:Region of Calcite deposition along section A-A' of Figure 4, scenario 3.

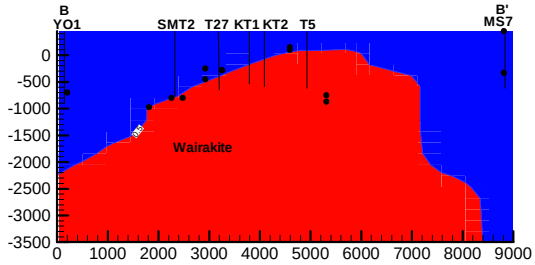

Figure 25:Region of Laumontite deposition along section A-A' of Figure 4, scenario 3. Solid circles represent estimated maximum depth of Laumontite alteration.

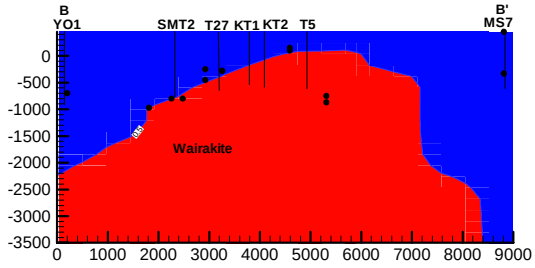

Figure 26:Region of Wairakite deposition along section A-A' of Figure 4, scenario 3

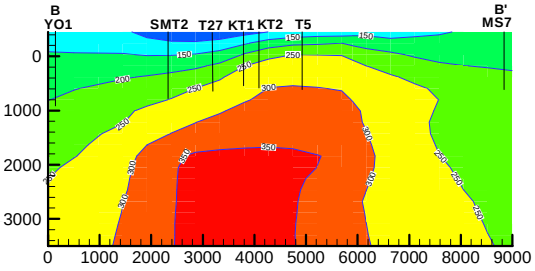

Figure 27:Temperature contours along section B-B'' of Figure 4, scenario 3.

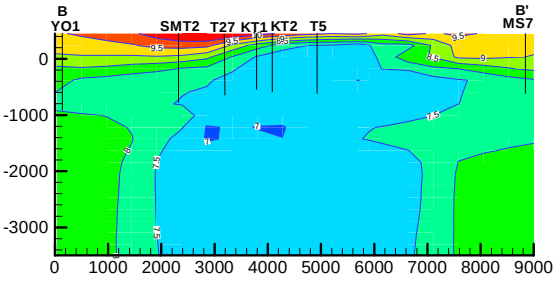

Figure 28:pH contours along section B-B' of Figure 4, scenario 3.

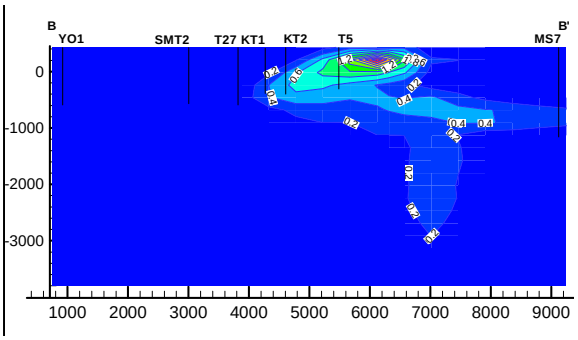

Figure 29: Location of Calcite deposition along section B-B'' of Figure 4, scenario 3.

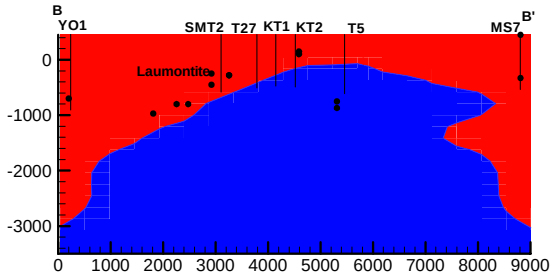

Figure 30: Location of Laumontite deposition along section B-B' of Figure 4, scenario 3. Solid circles represent estimated maximum depth of Laumontite alteration

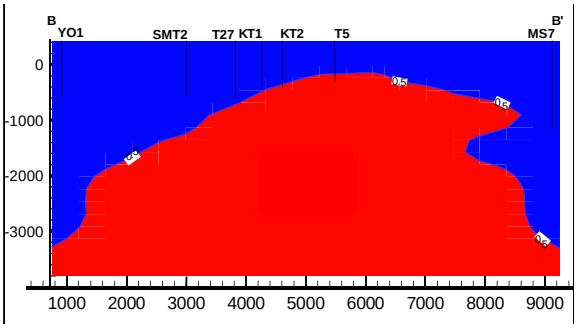

Figure 31: Location of Wairakite (red region) deposition along section B-B'' of Figure 4, scenario 2.

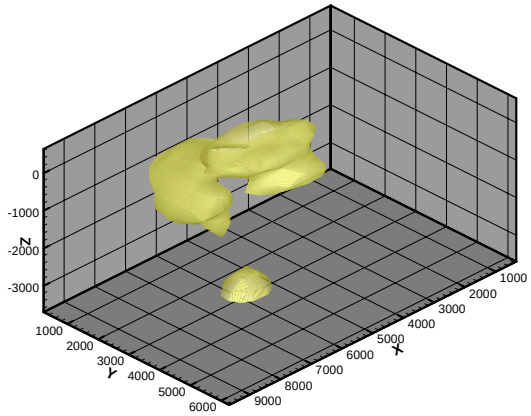

Figure 32: Location of Calcite deposition, scenario 3.

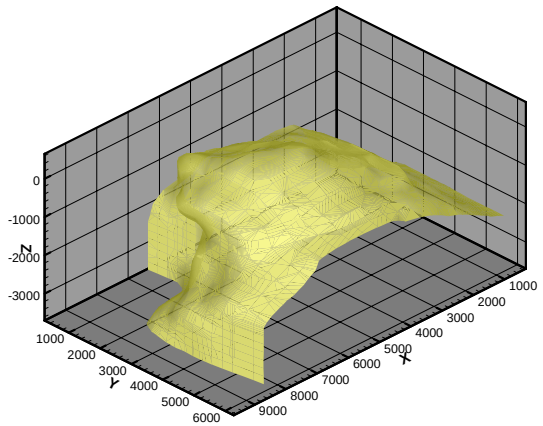

Figure 33: Lower surface of Laumontite, scenario 3.

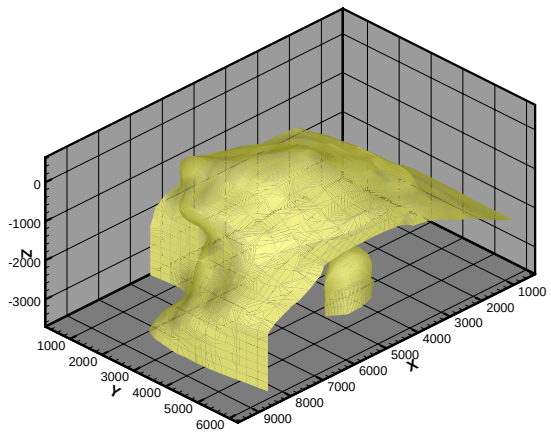

Figure 34: Upper and lower surfaces of Wairakite deposition, scenario 3.